Journal of Pharmaceutical and Medical Research
Print ISSN: 2663-1954
Online ISSN: 2663-1962
DOI: https://doi.org/10.61784/jpmr3100

RADIAL ONE-DIMENSIONAL HEAT AND MOISTURE COUPLING MODEL FOR THE PREHEATING STAGE OF HOT-AIR DRYING OF CYLINDRICAL MEDICINAL MATERIALS

XinLin Tu
College of Artificial Intelligence and Low-Altitude Technology, South China Agricultural University, Guangzhou 510642, Guangdong, China.

Abstract: This paper focuses on the preheating equilibrium stage in the hot-air drying process of cylindrical medicinal materials. A radial one-dimensional unsteady heat and moisture coupling model is established under the assumptions of axisymmetric and isotropic material. Heat transfer inside the material follows Fourier's law, moisture migration follows Fick's law, and the surface exchanges heat and moisture with the drying environment through convective transfer, which is described by third-kind boundary conditions. The measured drying-room temperature and moisture content are processed by piecewise linear interpolation and adopted as time-varying boundary conditions, and the governing equations are solved by an explicit finite difference scheme. During 0–1800 s, the material is heated as a whole while pre-drying occurs mainly in a thin surface layer. At 1800 s, the surface and center temperatures reach 36.79°C and 33.58°C, respectively. The surface moisture content decreases from 2.55 to 1.45 kg/kg on a dry basis, whereas the center moisture content remains close to its initial value. Convergence tests and parameter sensitivity analysis show that the surface temperature is most sensitive to the convective heat transfer coefficient, while the surface moisture content is most sensitive to the convective mass transfer coefficient and the diffusion pre-exponential factor.
Keywords: Hot-air drying; Heat and moisture coupling; Cylindrical medicinal material; Preheating equilibrium stage; Explicit finite difference

1 INTRODUCTION

Hot-air drying of cylindrical medicinal materials is a coupled heat and mass transfer process in which convective heat supply, internal conduction, and concentration-gradient-driven moisture migration jointly determine the spatiotemporal distributions of temperature and moisture content [1-2]. Because the axial dimension is typically much larger than the radial one, the radial direction dominates transport, making a reliable radial heat and moisture coupling model essential for understanding and optimizing the preheating equilibrium stage [3-4].

Considerable research has modeled coupled heat and mass transfer during convective drying. An implicit finite-difference method was applied to cylindrical moist objects, and the predicted instantaneous temperature and moisture distributions agreed well with experimental data [5]. Finite-element formulations have also been developed for cylindrical vegetable samples, showing that external resistance controls drying only when it is the rate-limiting step [6]. Microstructural characterization has recently been incorporated into transport modeling, and a microstructure-based transient model quantitatively revealed how a low-porosity surface layer impedes moisture diffusion and causes wet spots [7]. At the process scale, a transient CFD model under local thermal non-equilibrium theory was developed for thin-layer drying in a heat-pump dryer, achieving maximum relative errors of 11% for moisture and 3.58% for temperature [8]. Nevertheless, most existing models treat thermophysical properties as constant or focus on isothermal conditions [9]. Few have systematically addressed the preheating equilibrium stage, in which temperature and moisture fields evolve simultaneously under time-varying environmental conditions [10].

The present work establishes a radial one-dimensional heat and moisture coupling model for the preheating equilibrium stage of cylindrical medicinal materials. Third-kind boundary conditions are used for convective heat and moisture exchange, measured drying-room data are interpolated as time-varying boundary conditions, and an explicit finite difference scheme with verified stability and convergence yields the temperature and moisture distributions during 0–1800 s. The results provide a theoretical basis for subsequent modeling of the constant-temperature drying stage.

2 METHODOLOGY

2.1 Data Preprocessing

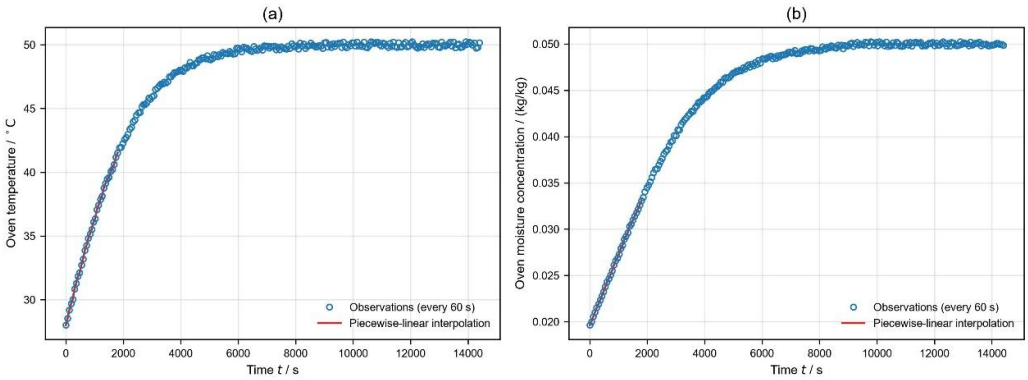
The required temporal resolution of environmental parameters is much higher than the sampling interval. Data interpolation must be performed before solving, and the interpolation method is described as follows. Piecewise linear interpolation is performed on the time series. Let two adjacent sampling points be (t_k, T_k) and (t_{k+1}, T_{k+1}). The drying room temperature T(t) at any time t between the two points is:

$$T(t) = T_k + \frac{T_{k+1}-T_k}{t_{k+1}-t_k}(t - t_k), \quad t \in [t_k, t_{k+1}] \tag{1}$$

© By the Author(s) 2026, under the CC BY-NC-ND license (http://creativecommons.org/licenses/by-nc-nd/4.0).

where T(t) denotes the drying room temperature at time t. The moisture concentration C(t) is interpolated using the same method. The nearest-neighbor extrapolation is adopted for values beyond the data range.

In the preheating stage, the drying room temperature gradually rises from 28°C to 50°C, and the moisture concentration increases from 0.0196kg/kg to 0.05kg/kg, providing external driving force for medicinal material heating and drying, as shown in Figure 1. Figure 1 presents the observed values and piecewise linear interpolation results of drying room temperature and moisture concentration. The interpolated curves fit well with observed points, indicating reasonable data preprocessing.



(a) Drying room temperature variation over time (b) Drying room moisture concentration variation over time

Figure 1 Environmental Parameters and Linear Interpolation of the Drying Room during Preheating Equilibrium Stage

2.2 Establishment of Transient Heat-Moisture Coupled Transfer Model

Heat and mass transfer occur simultaneously inside the medicinal material during the preheating equilibrium stage. This process is described by an axisymmetric cylindrical transient heat and moisture coupling model, as shown in Figure 2. The medicinal material is regarded as an axisymmetric cylinder; r denotes the radial distance to the medicinal material center, t denotes time. The internal temperature of the medicinal material is denoted as T(r, t), and the dry-base moisture concentration is denoted as C(r, t). The temperature follows the transient heat conduction law in cylindrical coordinates:

$$\rho c_p \frac{\partial T}{\partial t} = k\left(\frac{\partial^2 T}{\partial r^2} + \frac{1}{r}\frac{\partial T}{\partial r}\right) \tag{2}$$

where density $\rho = 820\text{kg/m}^3$, specific heat capacity $c_p = 2600\text{J/(kg}\cdot\text{K)}$, thermal conductivity $k = 0.36\text{W/(m}\cdot\text{K)}$. Figure 2 illustrates a schematic diagram of heat and moisture transfer in medicinal materials.

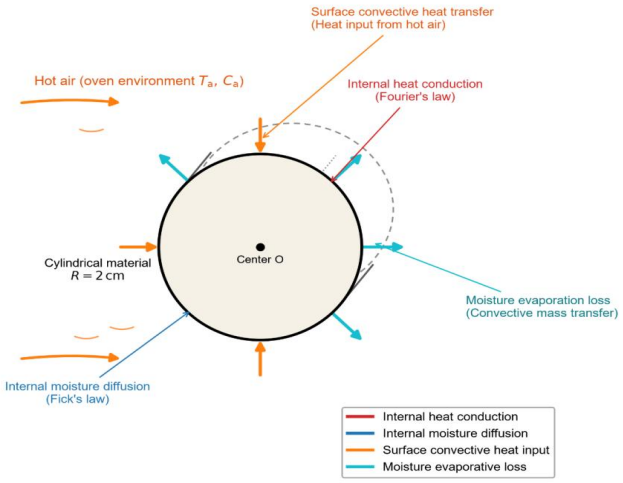


Figure 2 Schematic Diagram of Heat and Moisture Transfer in Medicinal Material

It should be noted that the internal moisture migration rate of medicinal materials is relatively slow in the preheating equilibrium stage, and the decrease of surface moisture concentration is limited. The latent heat taken away by water evaporation is much smaller than the convective heat transfer from the drying room to the medicinal material surface. Therefore, this paper neglects the influence of evaporation latent heat on the temperature field, and no phase-change latent heat source term is introduced into the temperature equation. This simplification is reasonable for the preheating equilibrium stage. The constant-temperature drying stage has a significantly increased water evaporation rate, so evaporation heat absorption cannot be neglected and a latent heat source term will be introduced into the energy equation.

Moisture migrates inside the medicinal material driven by concentration gradients. The moisture diffusion equation is written according to mass conservation:

$$\frac{\partial C}{\partial t} = D(C)\left(\frac{\partial^2 C}{\partial r^2} + \frac{1}{r}\frac{\partial C}{\partial r}\right) \tag{3}$$

The diffusion coefficient D varies with moisture concentration. In terms of boundary conditions, the axisymmetry at the medicinal material center r = 0 gives adiabatic and zero mass flux conditions:

$$\left.\frac{\partial T}{\partial r}\right|_{r=0} = 0, \quad \left.\frac{\partial C}{\partial r}\right|_{r=0} = 0 \tag{4}$$

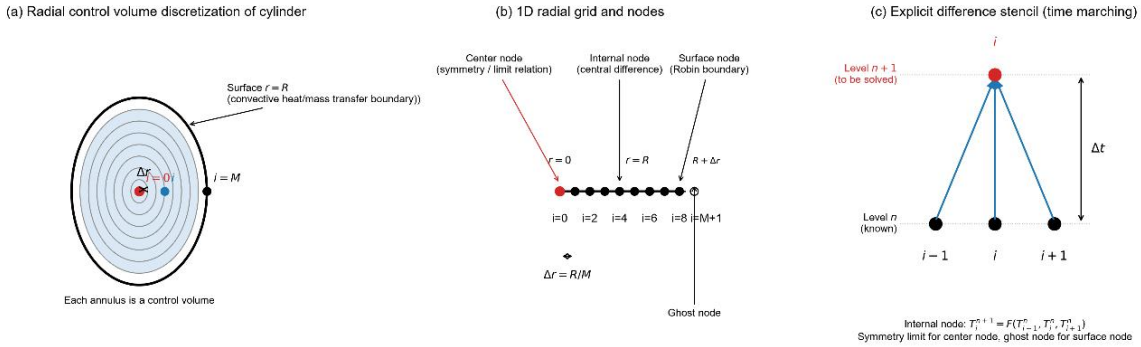
Convective heat transfer and convective mass transfer occur between the medicinal material surface and the drying room environment, and the boundary conditions are:

$$-k\left.\frac{\partial T}{\partial r}\right|_{r=R} = h[T(R,t) - T(t)], \tag{5}$$

$$-D\left.\frac{\partial C}{\partial r}\right|_{r=R} = \beta[C(R,t) - C(t)] \tag{6}$$

where the convective heat transfer coefficient h = 25W/(m^2 · K), and the convective mass transfer coefficient $\beta = 8 \times 10^{-7}$m/s. At the initial moment, the internal temperature and moisture concentration of the medicinal material are uniform:

$$T(r,0) = 28°C, C(r,0) = 2.55\ \text{kg/kg} \tag{7}$$



(a) Discretization of cylindrical radial control volume (b) Radial one-dimensional grid (c) Explicit difference template

Figure 3 Schematic Diagram of Explicit Finite Difference Discretization

The above equations are discretized using the explicit finite difference method, as shown in Figure 3. The radial direction is equally divided into M = 20 segments, with spatial step Δr = 0.001m and time step Δt = 1s. Let $r_i = i\Delta r$, $t^n = n\Delta t$. The node temperature and moisture concentration are denoted as T_i^n and C_i^n, respectively. For internal nodes (i = 1,2, . . . , M − 1), forward difference in time and central difference in space are adopted. The update formulas are:

$$T_i^{n+1} = T_i^n + \left(\frac{k}{\rho c_p}\right)\Delta t\left[\frac{T_{i+1}^n - 2T_i^n + T_{i-1}^n}{\Delta r^2} + \frac{T_{i+1}^n - T_{i-1}^n}{2r_i\Delta r}\right] \tag{8}$$

$$C_i^{n+1} = C_i^n + \Delta t[\quad D(C_i^n)\cdot\frac{C_{i+1}^n - 2C_i^n + C_{i-1}^n}{\Delta r^2} + D(C_i^n)\cdot\frac{C_{i+1}^n - C_{i-1}^n}{2r_i\Delta r} + \frac{D_{i+1} - D_{i-1}}{2\Delta r}\cdot\frac{C_{i+1}^n - C_{i-1}^n}{2\Delta r}] \tag{9}$$

For the center node (i = 0), using the limit relation:

$$\lim_{r\to 0}\left(\frac{\partial^2 T}{\partial r^2} + \frac{1}{r}\frac{\partial T}{\partial r}\right) = 2\frac{\partial^2 T}{\partial r^2} \tag{10}$$

This limit relation holds for both temperature field and moisture field. Combined with symmetry conditions $T_{-1}^n = T_1^n$, $C_{-1}^n = C_1^n$, the update formulas for the center node are:

$$T_0^{n+1} = T_0^n + 4\left(\frac{k}{\rho c_p}\right)\Delta t\frac{T_1^n - T_0^n}{\Delta r^2} \tag{11}$$

$$C_0^{n+1} = C_0^n + 4D(C_0^n)\Delta t\frac{C_1^n - C_0^n}{\Delta r^2} \tag{12}$$

Virtual nodes are introduced for surface nodes to rewrite the convective heat and mass transfer boundary conditions into explicit form. The virtual node values are:

$$T_0^{n+1} = T_0^n + 4\left(\frac{k}{\rho c_p}\right)\Delta t\frac{T_1^n - T_0^n}{\Delta r^2} \tag{13}$$

$$C_0^{n+1} = C_0^n + 4D(C_0^n)\Delta t\frac{C_1^n - C_0^n}{\Delta r^2} \tag{14}$$

Substitute the virtual node values back into the governing equations of surface nodes to obtain T_M^{n+1} and C_M^{n+1}. The stability conditions of the explicit scheme are:

$$\frac{k\Delta t}{\rho c_p \Delta r^2} \approx 0.17 < 0.5, \quad \frac{D_{\max}\Delta t}{\Delta r^2} \approx 0.494 < 0.5 \tag{15}$$

Both values are less than 0.5, satisfying stability requirements. Figure 3 shows a schematic diagram of the discretization using the explicit finite difference method.

3 RESULTS

The model is implemented in Python 3 with M = 20, Δr = 0.001m, and Δt = 1s. The solution is divided into four steps: first, interpolate the drying room temperature and moisture concentration onto the time grid with Δt = 1s; second, initialize the internal field of the medicinal material with T(r, 0) = 28°C and C(r, 0) = 2.55kg/kg; third, advance step by step in time, updating the temperature and moisture fields at each time step using the node difference formulas until t = 1800s; finally, output Table 1, Table 2 and complete result files.

3.1 Result Presentation

The temperature and moisture concentration results of the medicinal material within 30 minutes are shown in Table 1 and Table 2.

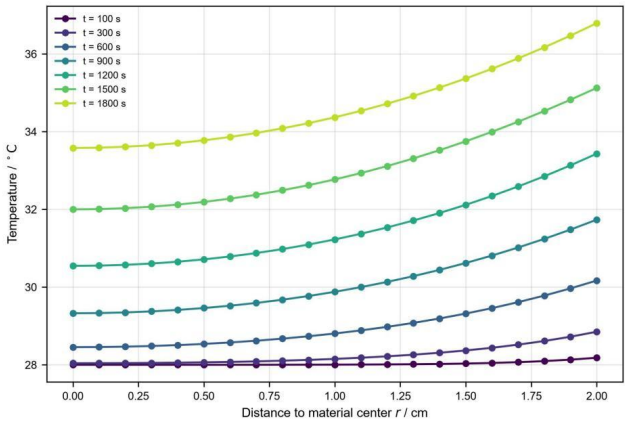


Figure 4 Radial Distribution of Medicinal Material Temperature at Different Moment

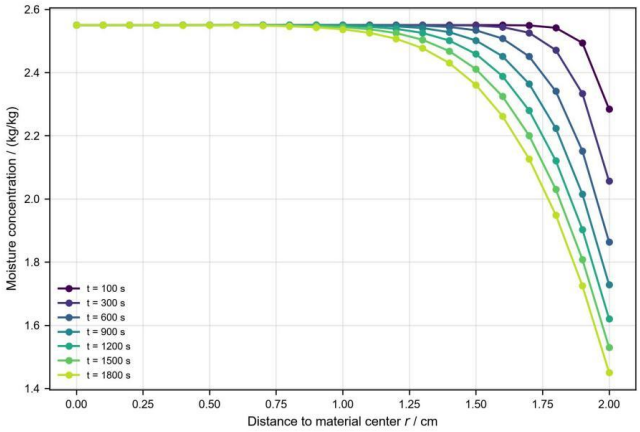


Figure 5 Radial Distribution of Medicinal Material Moisture Concentration at Different Moments

Table 1 Medicinal Material Temperature (°C) within 30 Minutes

Time/s	Distance to the center of medicinal material/cm				
	0	0.5	1	1.5	2
100	28.0001	28.0004	28.0041	28.0329	28.1810
300	28.0410	28.0638	28.1520	28.3692	28.8511
600	28.4545	28.5374	28.8056	29.3182	30.1683
900	29.3266	29.4606	29.8782	30.6194	31.7342
1200	30.5458	30.7130	31.2259	32.1165	33.4322
1500	31.9996	32.1907	32.7702	33.7507	35.1248
1800	33.5796	33.7763	34.3686	35.3668	36.7905

Table 2 Medicinal Material Moisture Concentration (kg/kg) within 30 Minutes

Time/s	Distance to the center of medicinal material/cm				
	0	0.5	1	1.5	2
100	2.5500	2.5500	2.5500	2.5500	2.2843
300	2.5500	2.5500	2.5500	2.5486	2.0559
600	2.5500	2.5500	2.5500	2.5335	1.8639
900	2.5500	2.5500	2.5495	2.5014	1.7285
1200	2.5500	2.5500	2.5477	2.4587	1.6206

Time/s	Distance to the center of medicinal material/cm				
1500	2.5500	2.5499	2.5436	2.4107	1.5297
1800	2.5500	2.5496	2.5367	2.3606	1.4506

To intuitively compare the radial differences inside the medicinal material at different moments, the radial distributions of temperature and moisture concentration at 100, 300, 600, 900, 1200, 1500 and 1800 s are plotted in Figure 4 and Figure 5. Figure 4 shows that the temperature curve rises as time proceeds, and the temperature difference between the center and surface gradually decreases. Figure 5 indicates that the surface moisture concentration decreases fastest, while the moisture concentration at the center barely changes. The moisture gradient is mainly concentrated in the thin layer near the surface.

3.2 Model Validation

Numerical convergence test. The center temperature, surface temperature and surface moisture concentration at t = 1800s are taken as observation indicators. The time and spatial steps are refined separately to observe changes in the results, as shown in Table 3 and Table 4.

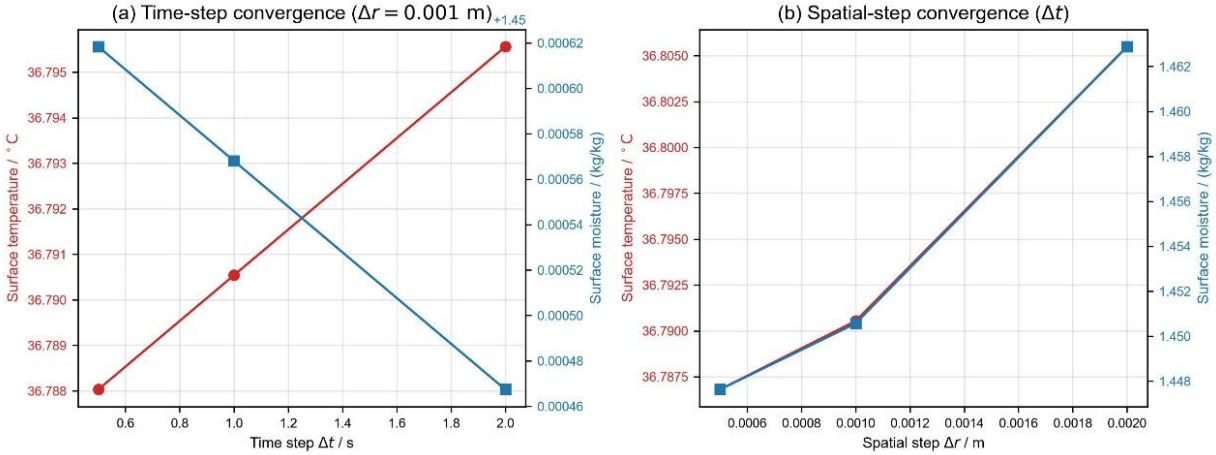
Table 3 Time Step Convergence Test

Time step Δt /s	Center temperature/ °C	Surface temperature/ °C	Center moisture/(kg/kg)	Surface moisture/(kg/kg)
2	33.5837	36.7956	2.5500	1.4505
1	33.5796	36.7905	2.5500	1.4506
0.5	33.5776	36.7880	2.5500	1.4506

Table 4 Spatial Step Convergence Test

Spatial step Δr /m	Center temperature/ °C	Surface temperature/ °C	Center moisture/(kg/kg)	Surface moisture/(kg/kg)
0.002	33.5925	36.8055	2.5499	1.4629
0.001	33.5796	36.7905	2.5500	1.4506
0.0005	33.5764	36.7868	2.5500	1.4476

The convergence curves are shown in Figure 6. Figure 6(a) shows time step convergence: when the time step is reduced from 1 s to 0.5 s, the surface temperature changes by about 0.007% and the surface moisture changes by about 0.003%. Figure 6(b) shows spatial step convergence: when the spatial step is refined from 0.001 m to 0.0005 m, the surface moisture changes by about 0.2%. The results demonstrate that the numerical solution is sufficiently convergent. Δt = 1s and Δr = 0.001m can guarantee four decimal places precision.



(a) Time step convergence (Δr = 0.001m) (b) Spatial step convergence (Δt = 1s)

Figure 6 Numerical Convergence Test

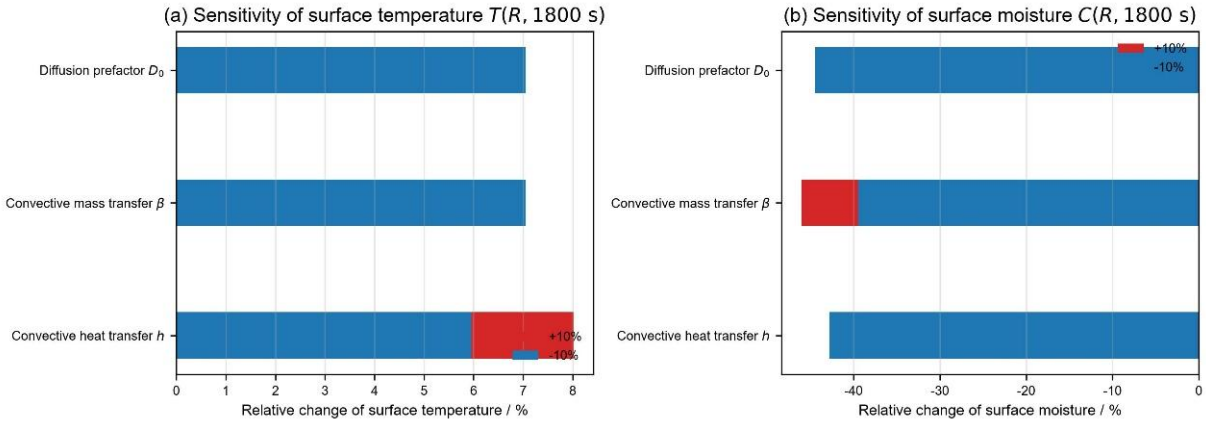
Parameter sensitivity analysis. Taking the surface temperature and surface moisture at t = 1800s as observation indicators, the convective heat transfer coefficient h, convective mass transfer coefficient β, and pre-factor of diffusion coefficient are increased and decreased by 10%, respectively. The results are shown in Table 5.

Table 5 Parameter Sensitivity Analysis

Parameter variation	Surface temperature/ °C	Relative temperature change	Surface moisture/(kg/kg)	Relative moisture change
h +10%	37.1208	+0.90%	1.4506	+0.00%

Parameter variation	Surface temperature/ ˚C	Relative temperature change	Surface moisture/(kg/kg)	Relative moisture change
h -10%	36.4135	-1.02%	1.4506	+0.00%
β +10%	36.7905	+0.00%	1.3693	-5.60%
β -10%	36.7905	+0.00%	1.5356	+5.86%
D_0 +10%	36.7905	+0.00%	1.4863	+2.46%
D_0 -10%	36.7905	+0.00%	1.4100	-2.80%

As shown in Table 5, the corresponding sensitivity responses are plotted in Figure 7. Figure 7(a) presents the sensitivity of surface temperature: surface temperature is sensitive to h. Figure 7(b) presents the sensitivity of surface moisture: surface moisture is most sensitive to β, followed by D_0. The elastic coefficients of the three parameters are all less than 1. The ±10 parameter perturbation will not be transmitted to the results at equal magnitude, indicating that the model has good robustness.



(a) Sensitivity of surface temperature (b) Sensitivity of surface moisture concentration

Figure 7 Responses of Surface Temperature and Surface Moisture under ±10 Perturbation of Model Parameters

Axisymmetric transient heat and moisture transfer partial differential equations are established for the preheating equilibrium stage, and solved by explicit finite difference method up to t = 1800s. At this moment, the surface temperature is 36.79°C, the center temperature is 33.58°C, and the surface moisture content decreases from 2.55kg/kg to 1.4506kg/kg. The whole process features overall temperature rise and pre-drying in the thin surface layer; moisture decreases obviously only near the surface. The model passes convergence test and parameter sensitivity analysis.

4 CONCLUSIONS

This paper constructs a radial one-dimensional transient heat-moisture coupling model for the preheating-equilibrium stage of hot-air drying of cylindrical medicinal materials. With axisymmetric and isotropic assumptions, Fourier's heat conduction law and Fick's moisture diffusion law are adopted, and time-variant environmental boundary conditions are obtained via piecewise-linear interpolation of actual drying-room measurement data. An explicit finite-difference scheme is used to solve the governing partial-differential equations. Numerical results reveal that within 0-1800 s, the medicinal material undergoes overall temperature rise, while moisture reduction is concentrated in the near-surface thin layer. At 1800 s, the surface temperature reaches 36.79 °C and the center temperature is 33.58 °C; surface dry-basis moisture falls from 2.55 kg/kg to 1.45 kg/kg, whereas central moisture barely changes. Convergence tests verify the rationality of selected spatial-temporal discretization parameters, and parameter-sensitivity analysis demonstrates that convective heat-transfer coefficient dominates surface temperature response and convective mass-transfer coefficient dominates surface moisture variation. The proposed model can realize fast numerical prediction of temperature-moisture distribution in the preheating phase, and it is applicable for pre-evaluation of process parameters for cylindrical-medicinal-material hot-air drying.

Nevertheless, the present work only focuses on the preheating-equilibrium stage and ignores the latent-heat effect of water evaporation in this phase for simplification. In future research, evaporation latent-heat source terms will be supplemented to establish a full-stage heat-moisture coupling model covering both preheating and constant-temperature drying periods. Temperature- and moisture-dependent thermophysical properties will be introduced, and two-dimensional axial-radial numerical models will be developed. Further work will combine experimental drying data for model calibration and validation, so as to provide more accurate simulation support for practical medicinal-material drying-process optimization.

COMPETING INTERESTS

The authors have no relevant financial or non-financial interests to disclose.

REFERENCES

[1] Beheshti R, Pakkhesal S, Naseri A, et al. Efficacy of Herbal Medicine on Cognitive Function in Multiple Sclerosis: A Systematic Review and Network Meta-Analysis. Multiple Sclerosis and Related Disorders, 2026, 114(S1): 107489.
[2] Gyamfi A S, Agyemang O K, Nkrumah E E, et al. The Intersection of Christianity and Herbal Medicine Practices Among the Asante of Ghana. Society, 2026: 1-14.
[3] Yang J, Zhan J, Wang W, et al. Traditional Chinese Medicine in the Treatment of Membranous Nephropathy: Therapeutic Effects and Mechanistic Insights. Seminars in Nephrology, 2026: 151714.
[4] Shahrezaei A, Taherkhani S, Dashti L, et al. Herbal medicine meets machine learning: a systematic review of AI-powered innovation in chronic inflammation management. Discover Applied Sciences, 2025, 8(2): 111.
[5] Antunes M D M, Burgers I, Ozenne V, et al. New analytical and hybrid heat transfer models for thermal ablation procedures validated by MRI thermometry. International Journal of Hyperthermia, 2025, 42(1): 2594943.
[6] Wang G, Zhang M, Huang J, et al. Parameter identification of condenser heat transfer model based on improved flower pollination algorithm. Scientific Reports, 2025, 15(1): 39310.
[7] Jiang Y, Hong Y, Su X, et al. Study on the Control Effect of Chinese Herbal Medicine Regulator on Leaf Spot Nematode Disease of Chloranthus spicatus. Agricultural Biotechnology, 2024, 13(6): 92-98, 101.
[8] Ahmed A L, Hussain A, Barbhuiya A P, et al. Herbal Medicine for the Management of Wounds: A Systematic Review of Clinical Studies. Infectious Disorders Drug Targets, 2024, 25(5): e18715265320593.
[9] Awwad O, Saleh M, Bardaweel S, et al. Use of complementary and alternative medicine among females with polycystic ovary syndrome in Jordan: a cross-sectional study. BMJ Open, 2024, 14(12): e088945.
[10] Fu Y, Yang S, Qiao X. Heat transfer analysis and optimization of service based on unsteady heat transfer model. Frontiers in Power and Energy Systems, 2024, 3(1).